Journal Name

Dynamic Article Links ►

Cite this: DOI: 10.1039/c0xx00000x

www.rsc.org/xxxxxx

ARTICLE TYPE

Hyperbranched Crystalline Nanostructure Produced from Ionic π-Conjugated Molecules†

Jeremy R. Eskelsen [a], Kara J. Phillips,[b] K. W. Hipps,[a]* and Ursula Mazur[a]*

Chem Comm 2014 DOI: 10.1039/C4CC09288K

Self-assembled crystalline nanostructures with sheaf-like morphology fabricated from tetra(4-aminophenyl)porphyrin and tetra(4-sulfonatophenyl)porphyrin are reported for the first time. The hierarchical sheaf-like growth of the assemblies exhibits Arrhenius behaviour. The observed morphology results from crystal splitting during initial oriented attachment growth followed by Ostwald ripening.

The fabrication of well-ordered multidimensional nano and microstructured optoelectronic materials continues to be the subject of intense research because of their increasing use in applications such as sensing,[1] catalysis,[2] and energy conversion and storage.[3-5] Three dimensional (3D) assemblies are generally preferred over their 1D and 2D counterparts since the enlarged specific surface area is advantageous for enhanced performance of sensors and catalysts where the number of active sites scales with the available surface area. For high efficiency of solar to electrical energy conversion, the high surface to volume ratio of nanostructured electrodes provides short electrical pathways for rapid transport and efficient collection of carriers throughout the device.

Recently, efforts have been focused on the synthesis of complex 3D hierarchical crystalline nanoarchitectures using low dimensionality building blocks composed of wires, rods, and fibers. In this approach, the growth of 1D and 2D elements proceeds in both axial and lateral directions resulting in well-defined branched/hyperbranched 3D structures that possess a high degree of connective complexity.[6-9] The benefits of higher connective density of branched nanostructures (fabricated from inorganic semiconductors, primarily metal oxides[1,8,10] and chalcogenides[11,12]) have been demonstrated for photovoltaics,[8,] sensing,[1,10] photocatalysis,[3] photoelectrochemical water splitting,[13] supercapacitors,[14] and batteries.[15]

Electroactive organic compounds are viable alternatives to inorganic semiconductors with the advantage of having their optical and electrical properties chemically tuned by molecular design. 1D and 2D crystalline nanostructures fabricated from π-conjugated molecules are quite common.[16-18] 3D branched conductive polymers (dendrimers) are also known and can be prepared with high regularity and controlled molecular weights but their morphology is not always well defined.[19,20] An interesting class of highly conjugated organics with demonstrated potential for growing multidimensional crystalline nanostructures

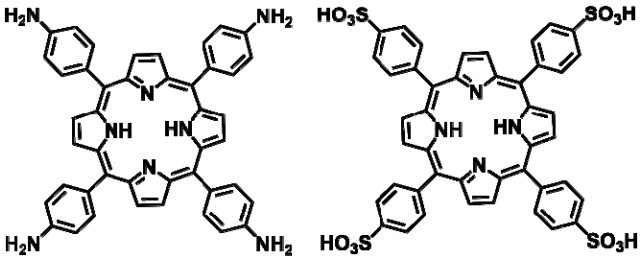

Fig. 1 Left – tetra(4-aminophenyl)porphyrin (TAPP), right – tetra(4-sulfonatophenyl)porphyrin (TSPP).

are porphyrins.[21,22,23] Porphyrins structurally and functionally resemble natural light-harvesting chromophores and can serve as light-harvesting components in dye-sensitized solar cells and organic photovoltaics.[23,24,25] In addition, the mechanical properties of 1D crystalline porphyrin nanostructures are comparable to those of polymeric systems making them excellent candidates for flexible optoelectronic devices.[26]

Here, we report the first crystalline hyperbranched 3D nanostructure fabricated from porphyrins with well-defined sheaf-like morphology. They structurally emulate the hyperbranched structures made from inorganics (e.g. α-Fe_2O_3,[1] α-GaOOH,[10] Bi_2S_3,[12] and CuO[27]). We propose a crystal growth mechanism for the porphyrin-based nanosheaves and evaluate the growth kinetics. These factors play a fundamental role in determining the size and morphology of the nanostructure.

The 3D porphyrin nanostructures were prepared by ionic self-assembly[23,26-29] from metal free porphyrin tectons, meso-tetra(4-aminophenyl)porphyrin, TAPP and meso-tetra(4-sulfonatophenyl)porphyrin, TSPP (Fig. 1). The TAPP:TSPP nanoassemblies were formed reproducibly in a 1:1 stoichiometric porphyrin ratio in a pH 3 aqueous solution (see ESI for details of the synthesis). At this hydrogen ion concentration, the expected charges on the TAPP and TSPP ions are +2 and -2, respectively.[30,31] The morphology of the nanostructures was characterized using atomic force microscopy (AFM) and high resolution transmission electron microscopy (HRTEM). Selected area electron diffraction (SAED) and powder X-ray diffraction (XRD) helped to deduce the structure and organization of porphyrin molecules within the nanoassemblies. The effects of reaction temperature and time as well as solution concentration on the growth of these nanostructures were also investigated.

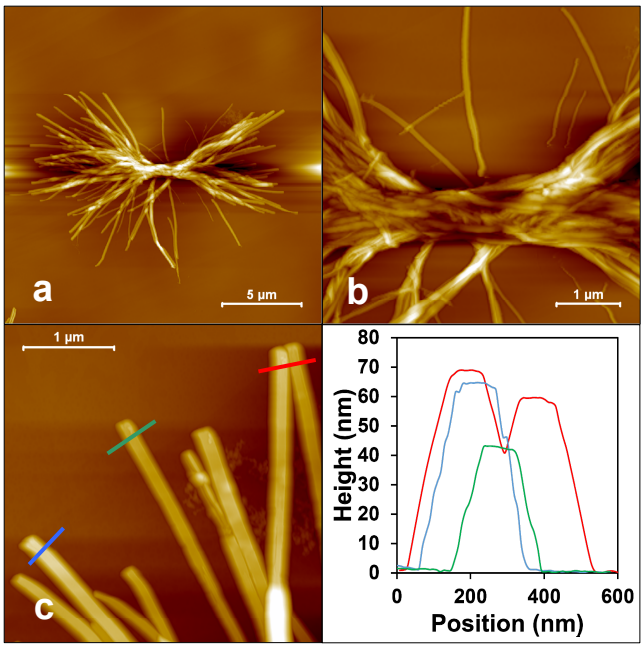

Fig. 2 Tapping mode AFM images of TAPP: TSPP nanosheaves prepared from equimolar (5µM) porphyrin solutions at pH 3 and 75 °C: (a) single sheave, (b) sheave core, and (c) sheave ribbons and associated cross sectional profile (right). Samples were deposited onto highly ordered pyrolytic graphite. Images were acquired under ambient conditions.

Synthesized as described, TAPP:TSPP nanostructures exhibit sheaf-like morphology composed of ribbon filaments, uniform in size, branching out from a single core as depicted in the low resolution AFM image in Fig. 2a. The core of the sheaf is composed of a bundle of intercrossing ribbons with no clear definition of the growth origin (Fig. 2b). In all of our preparations of the TAPP:TSPP assemblies we only observed double-sheaf growth having only two growth cones oriented at 180° relative to each other. A single sheaf bundle consists of ribbons 50 nm tall and 180 nm wide. The width of the TAPP:TSPP nanofiber is almost identical to the reported 170 nm diameter of a GaOOH[10] nanofilament. The individual TAPP:TSPP nanoribbons are uniform in width with squared ends and flat and smooth tops. The length of the nanoribbons measured from the center of the bundle (half-length) is approximately 7 µm, about twice as larger as hyperbranched sheaf-like GaOOH nanoassemblies.[10]

High-resolution TEM micrographs of the TAPP:TSPP nanostructures prepared at 75 °C exhibit clear lattice fringes 1.4 nm apart (Fig. 3a). Samples prepared at lower temperatures were also crystalline. Electron diffraction images of the same sample acquired sequentially starting at the terminus and following along a single nanoribbon reveal that the molecular sheaves are homogeneously single-crystalline. An example image in Fig. 3b shows a spot pattern indicating a high degree of molecular ordering in the TAPP:TSPP sheaves. The diffraction patterns are consistent with a body centered crystal system due to the presence of 200, 002, and 510 and the absence of 210 diffraction spots. Table S1, in ESI, shows electron diffraction spacings in the *a* and *c* directions calculated based on a body-centered orthorhombic crystal. The average distances are $a = 31.3 \pm 0.8$ Å and $c = 8.0 \pm 0.2$ Å with $\alpha = \beta = \gamma = 90°$. These distances agree well with spacings observed by X-ray diffraction, Fig. S3 in ESI. The 1.4 ± 0.14 nm spacing observed by HRTEM corresponds with *a*/2 or the distance in the [200] direction. We did not observe the spacings in the *b* direction by TEM because the nanoribbons lie preferentially on the (020) face in contact with the TEM grid surface. This orientation is different from that of 1D porphyrin nanostructures fabricated from tetra(4-pyridyl) porphyrin (TPyP) and tetra(4-sulfonatophenyl)porphyrin (TSPP). The TPyP:TSPP nanorods lie preferentially with the (110) face parallel to the substrate surface.[26] In the TPyP:TSPP nanorods, the ionic tectons alternate in a face-to-face arrangement forming columns along the length of the nanorods.[26] The stacked chromophores are held together by electrostatic and π-π interactions and the columnar chains are held together primarily by hydrogen bonding. We expect similar intermolecular interactions to direct the structure of the TAPP:TSPP ribbons in the sheaves.

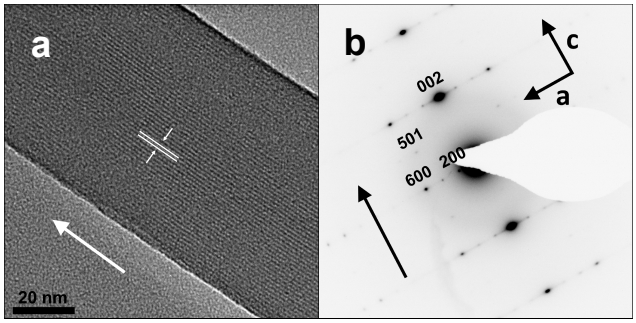

Fig. 3 HRTEM of a TAPP: TSPP nanoribbon showing lattice fringes (a). These spacings identified with parallel bars are similar to those observed by powder XRD for the 200 and 110 directions. SAED of the same sample is shown in (b). Here, the image color is inverted for clarity. The fastest growth direction in both (a) and (b) is indicated by the long arrows. Porphyrin solid was prepared at 75 °C.

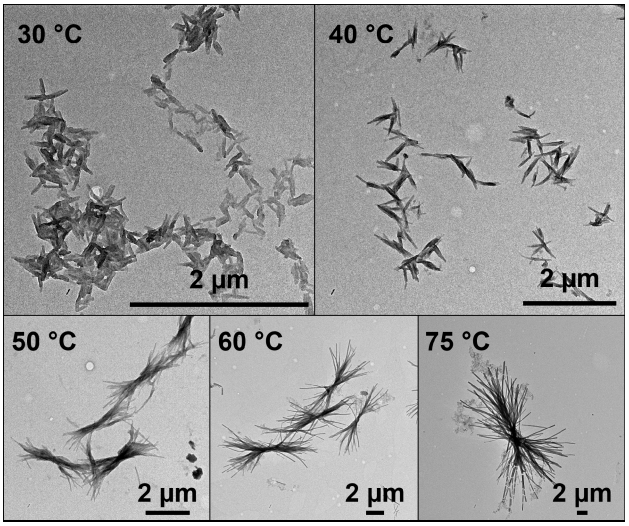

Fig. 4 TEM micrographs showing the temperature dependent growth of TAPP:TSPP structures made from equimolar (5 µM) porphyrin solutions at pH 3. Small rods are observed at low temperatures. With increasing temperature the petite rods appear to split and grow forming sheaves with long ribbons.

In order to better understand the formation of the sheaf-like structures we examined their growth as a function of temperature, time, and tecton concentration. TEM images of TAPP:TSPP samples prepared at temperatures ranging from 30 °C to 75 °C are depicted in Fig. 4. At low temperatures only short rods approximately 300 nm long are produced. Higher reaction temperatures favor larger structures with greater number of branches. A plot of the nanostructure lateral growth as a function of temperature exhibits an Arrhenius behavior, $L_{1/2}(T) = A \exp(-E_a/k_BT)$ which is summarized in Fig. 5. Here, the half-length

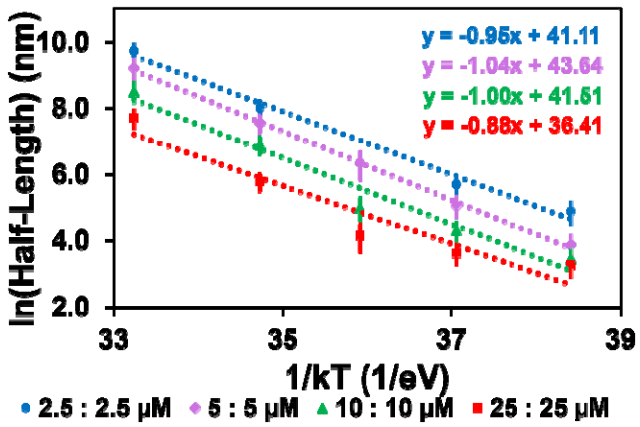

Fig. 5 Plot showing the Arrhenius-like dependence of the TAPP:TSPP sheaf half-length on temperature (30°C -75 °C).

($L_{1/2}$) is the length measured from the center of the sheave to the tips of the nanoribbons collected from multiple TEM images in multiple experiments, E_a is an energy barrier related to the crystal growth, k_B is Boltzmann's constant in eV/K, and T is the reaction temperature. Typically the value of E_a is derived from the kinetic constants as a function of temperature. Since we are using the half-length to calculate E_a we assume the crystal growth has reached an asymptotic value and the value of E_a obtained is the average of all growth processes occurring in the closed system. The stoichiometric concentration of the TAPP and TSPP solutions employed varied from 2.5 μM to 25 μM. The slope of the linear fit of the ln($L_{1/2}$) versus $1/kT$ plot suggests an energy barrier (E_a) of 0.97±0.04 eV (93 ± 5 kJ/mol). The magnitude of this activation barrier is indicative of an integration controlled crystal growth as the energies associated with this type of processes are typically >40 kJ/mol.[32] Activation energies in diffusion controlled growth are much lower. [32]

Time dependent growth of TAPP:TSPP sheaves was also studied. By pipetteing an aliquot of a heated (75 °C) stoichiometric TAPP:TSPP mixture at different reaction time intervals onto a chilled TEM grid we monitored the crystal growth process. These samples provided us with 'snapshots' of how the nanostructure develops at reaction times ranging 4-30 minutes (Fig. S7 in ESI). After 4 min we observed the formation of 2 μm sheaf-like bundles that progressively grew larger with increasing number of ribbons per sheaf. After 30 min the sheaves were 12 μm in length. Fig. 6 depicts the a fit of the time dependent sheave growth of TAPP:TSPP based on LSW classical kinetic model for crystal coarsening (Ostwald ripening, OR).[33-36]

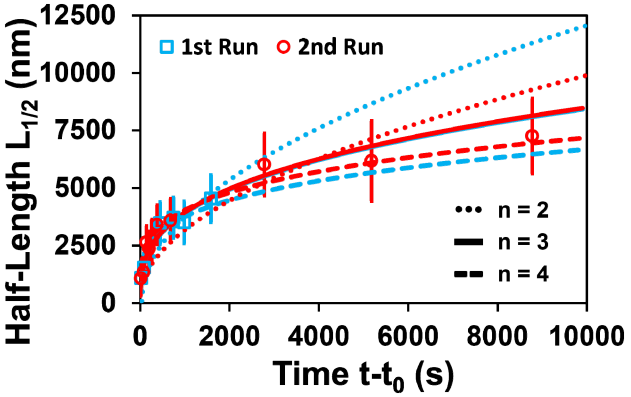

Fig. 6 Time dependent growth of TAPP:TSPP nanoribbons ($L_{1/2}$) versus time (sec) fit to the LSW classical kinetic model for crystal coarsening. Fits for different values of n are shown for n = 2 (dotted line), n = 3 (solid line), n = 4 (dashed line).

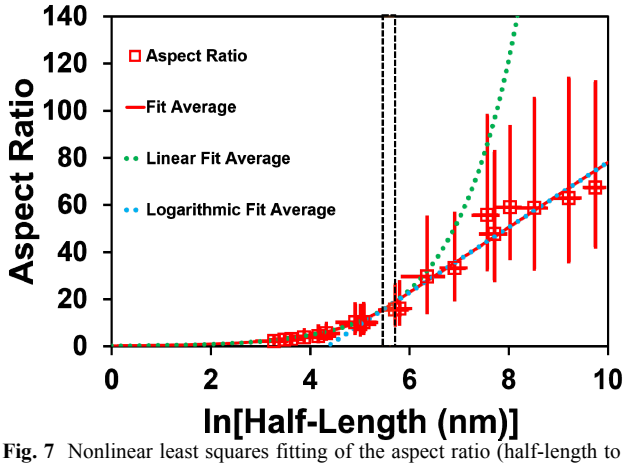

Fig. 7 Nonlinear least squares fitting of the aspect ratio (half-length to width quotient) versus the ln($L_{1/2}$), where $L_{1/2}$ is the half length of the nanofibers. The vertical bar marks a transition region from the linear to the logarithmic fit.

A generalized equation of the LSW model is: $R = [k(t - t_0) + R_0^n]^{1/n}$, where R and R_0 are the mean sheaf half-length at time t and t_0 respectively, and k and n are considered as characteristic of the particle growth mechanism. Experimentally n has been found to vary from 1 to 10 although only values between 1 and 4 are considered to have any physical meaning (dimensionality).[36,37] Using the LSW equation we obtained the best fit of our time-dependent TAPP:TSPP growth data (within experimental error) using n values of 3 and 4 along with refinement of R_0, t_0, and k. The value of t_0 is about 100 ± 50 s for these values of n. R_0 is susceptible to parameterization and varied from of 20 to 300 nm for the different estimates of k and R_0, and n values employed. The value of k was 6.0 (± 0.2) x 10^7 s^{-1} for n = 3 and 2.0 (± 0.1) x 10^{11} s^{-1} for n = 4. This growth is much faster than OR growth reported for inorganic materials.[10,12,27,36]

A plot of the aspect ratio of the TAPP:TSPP nanoribbons (half-length to width quotient) against the ln(half-length) is depicted in Fig. 7. This curve can be satisfactorily modeled with nonlinear least squares fitting using the Levenberg-Marquardt method in MathCAD 14, where the error on the residuals is minimized (see ESI for details). A combination of a linear segment and an exponential segment intersect in approximately 250-300 nm region which is close to our particle radius R_0 upper bound value (300 nm) obtained from the time dependent growth experiments (Fig. 6). This dimensional transition may be attributed to change from an oriented attachment (OA) growth mechanism to the OR controlled growth. OA mechanism is frequently applied to nanocrystal growth, where nanoparticles with matching crystallographic orientations directly combine together to form larger ones.[10,12,27,36] Mixed OA and OR growth mechanisms were reported for nanocrystalline systems like α-GaOOH,[10] Bi_2S_3,[12] and ZnS.[38] In the case of TAPP:TSPP growth, the OR mechanisms likely dominates the long term growth of individual nanoribbons. This is supported by our time dependent data.

It is generally accepted that 3D sheave structures result from a crystal splitting growth mechanism.[6] Crystal splitting is associated with fast crystal growth but can also result from defects and stresses. [6] In the case of hyperbranched TAPP:TSPP we propose the following scenario. Initially porphyrin dimers aggregate or self-assemble into crystalline nanoparticles and proceed via oriented attachment to form larger nanocrystals to minimize surface energy. During the continuous growth of the TAPP:TSPP nanoribbons, porphyrin dimers preferentially adsorb on the end of the nanowires rather than the center. This growth progresses along the c-axis of the TAPP:TSPP orthorhombic

structure, or the [002] direction. The growth direction is consistent with the aspect ratio vs. the half-length of the nanoribbon shown in Fig. 7.

It is likely that the initial OA growth produces defects and lattice mismatch along the slow growth (attachment) faces. These defects may cause the crystal splitting seen in the fully developed sheaf. The splitting would most likely occur along the (100) and (010) planes in the starting TAPP:TSPP nuclei where weak hydrogen bonding interactions hold the face-to-face stacked porphyrin columns together. Orthorhombic α-GaOOH[12] and Bi_2S_3[10] sheaves are also composed of chainlike crystalline structures along the length of the crystal fibers. It was proposed that crystal splitting in these inorganic structures was due to weak interactions between adjacent chains. After crystal splitting in the TAPP:TSPP (i.e. the region of growth around 300 nm, based on the time-dependent and aspect-ratio data, figures 6 and 7, respectively) OR growth dominates resulting in smooth nanoribbons with squared off ends (as per the AFM images, Fig 2). Shortly, we will study the TAPP:TSPP nanostructure growth in-situ using STEM (scanning TEM) imaging under continuous flow conditions. This method will allow us to image both the products and the reactants in real time and help us better understand the dynamics of growing the TAPP:TSPP hyperbranched structures.

In summary, we report the first ionic organic nanocrystal exhibiting a sheaf-like structure that bears very close morphological and dimensional resemblance to inorganic hyperbranched nanostructures. TAPP:TSPP sheaves with stoichiometric porphyrin composition are orthorhombic single crystals with a face-to-face stacking of porphyrin tectons. The overall size of the nanostructures can be tuned by controlling the reaction temperature and initial concentration. The formation of the sheaf-like structures is the result of crystal splitting of a cluster of coalesced nanorods formed during an initial OA growth period followed by the long term growth of individual nanoribbons via OR mechanisms. The growth of the TAPP:TSPP nanosheaves follows an Arrhenius dependence with an activation energy of 93±5 kJ mol^{-1}. We currently are examining the potential optical and chemical sensing properties of these high surface area hyperbranched porphyrin nanostructures.

This material is based upon work supported by the National Science Foundation CHE-1152951. KP thanks NSF-REU Program DMR-1062898 for funding. We express our gratitude to the Francheschi Microscopy and Imaging Center at Washington State University for the use of their transmission electron microscopes.

Notes and references

[a] Department of Chemistry, Washington State University, Pullman, WA 99164-4630, USA.
[b] Department of Chemical Engineering and Materials Science, University of California, Irvine, California 92697-2700

†Electronic supplementary information (ESI) is available. For ESI including sample preparation, electronic spectra, x-ray diffraction and additional TEM data see DOI: 10.1039/c000000x/

1 P. Sun, S. Du, T. Yang, X. Li, F. Liu, X. Liang, Y. Gao, Y. Sun, and G. Lu, *RSC Advances*, 2013, **3**, 7112-7118.
2 Z. Jia, L. Yang, Q. Wang, J. Liu, M. Ye, and R. Zhu, *Mater. Chem. Phys.*, 2014, **145**, 116-124.
3 Q. Liu, Y. Zhou, Z. Tian, X. Chen, J. Gao, and Z. Zou, *J. Mater. Chem.*, 2012, **22**, 2033-2038.
4 Y. Tian, K. E. Martin, J. Y.-T. Shelnutt, L. Evans, T. Busani, J. E. Miller, C. J. Medforth, and J. A. Shelnutt, *ChemCommun.*, 2011, **47**, 6069-6071.
5 J. Bai, X. Li, G. Liu, Y. Qian, and S. Xiong, *Adv. Funct. Mater.*, 2014, **24**, 3012-3020.
6 C. Cheng and H. J. Fan, *Nano Today*, 2012, **7**, 327-343.
7 H. Li, A. G. Kanaras, and L. Manna, *Acc. Chem. Res.*, 2013, **46**, 1387–1396.
8 L. Passoni, F. Ghods, P. Docampo, A. Abrusci, J. Marti-Rujas, M. Ghidelli, G. Divitini, C. Ducati, M. Binda, S. Guarnera, A. Li Bassi, C.S. Casari, H.J. Snaith, A. Petrozza, and F. Di Fonzo, *ACSNano*, 2013, **7**, 10023–10031.
9 H. Zhou and Z. R.Tian, *Prog. Nat. Sci.: Mat. Inter.*, 2013, **23**, 273-285.
10 S. Wu, J. Zhang, L. Shi, S. Tang, Y. Li, L. Jiang, and Q. Cui, *RSC Adv.*, 2014, **4**, 8209–8215
11 H. Zhang, D.-H. Ha, R. Hovden, L. F. Kourkoutis, and R. D. Robinson, *Nano Lett.*, 2011, **11**, 188–197.
12 J. Tang and A.P. Alivisatos, *Nano Lett.*, 2006, **6**, 2701-2706.
13 K.X. Wang, Z. Yu, V. Liu, M.L. Brongersma, T. F. Jaramillo, and S. Fan, *ACS Photonics*, 2014, **1**, 235-240.
14 Q. Yang, Z. Lu, J. Liun, X. Lei, Z. Chang, L. Luo, and X. Sun, *Prog. Nat. Sci.: Mat. Inter.*, 2013, **23**, 351–366.
15 Y. Zhang, L. Guo, and S. Yang, *Chem. Commun.*, 2014, **50**, 14029-14032.
16 L. Zang, Y. Che, and J. S. Moore, *Acc. Chem. Res.*, 2008, **41**, 1596-1608.
17 A. Borras, O. Groning, M. Aguirre, F. Gramm, and P. Groning, *Langmuir*, 2010, **26**, 5763-5771.
18 H. Yu, D. Y. Kim, K. J. Lee, and J. H. Oh, *J. Nanosci. Nanotech.*, 2014, **14**, 1282–1302.
19 D. Astruc, E. Boisselier, and C. Ornelas, *Chem. Rev.*, 2010, **110**, 1857–1959.
20 K. Inoue, *Prog. Polym. Sci.*, 2000, **25**, 453-571.
21 B. A. Friesen, B. Wiggins, J. L. McHale, U. Mazur, and K. W. Hipps, *J. Phys. Chem. C*., 2011, **115**, 3990-3999.
22 Y. Tian, T. Busani, G. H. Uyeda, K. E. Martin, F. van Swol, C.J. Medforth, G. A. Montano, and J. A. Shelnutt, *Chem. Commun.*, 2012, **48**, 4863–4865.
23 J. A. Shelnutt, Y. Tian, K. E. Martin, and C. J. Medforth, in *Handbook of Porphyrin Science*, eds. K. M. Kadish, K. M. Smith, and R. Guilard, 2014, World Scientific Publishing Co., Hackensack, NJ, vol. 28, pp. 227-277.
24 M. Vasilopoulou, D. G. Georgiadou, A. M. Douvas, A. Soultati, V. Constantoudis, D. Davazoglou, S. Gardelis, L.C. Palilis, M. Fakis, S. Kennou, A. G. Lazarides, A. G. Coutsolelosd, and P. Argitis, *Mater. Chem. A*, 2014, **2**, 182–192.
25 P. Guo, P. Chen, M. Ma, and L. Liu, *J. Mater. Chem.*, 2012, **22**, 20243-20249.
26 J. R. Eskelsen, Y. Qi, S. Schneider-Pollack, S. Schmitt, K. W. Hipps, and U. Mazur, *Nanoscale*, **2014**, 6, 316-327.
27 Y. Zhao, H, Shi, M. Chen, and F. Teng, *CrystEngComm,* 2014, **16**, 2417-2423.
28 A. D. Schwab, D. E. Smith, C. S. Rich, E. R. Young, W. F. Smith, and J. C. de Paula, *J. Phys. Chem. B*, 2003, **107**, 11339–11345.
29 J. R. Eskelsen, Y. Wang, Y. Qi, M. Ray, M. Handlin, K. W. Hipps, and U. Mazur, *J. Porph. Phthal.*, 2012, **16**, 1233–1243.
30 C. Wang and C. C. Wamser, *J. Phys. Chem. A*, 2014, **118**, 3605-3615.
31 A. Farjtabar and F. Gharib, *J. Solution Chem.*, 2010, **39**, 231-244.
32 *Measurement of crystal Growth and Nucleation Rates,* eds. J. Garsie, S. Mersmann, and J. Nyvit, 2002, Institution of Chemical Engineers., UK, pp. 24.
33 I. M. Lifshitz and V. V. Slyozov, *J. Phys. Chem. Solids*, 1961, **19**, 35-50.
34 C. Wagner, *Z. Elektrochemie*, 1961, **65**, 581-591.
35 M. Kahlweit, *Adv. Colloid Interface Sci.*, 1975, **5**, 1-35.
36 J. Zhang, F. Huang, and Z. Lin, *Nanoscale*, 2010, **2**, 18–34.
37 N. Daneu, A. Recnik, and S. Bernik. *J. Am. Ceram. Soc.*, 2011, **94**, 1619-1626.
38 F. Huang, H. Zhang, and J. F. Banfield, *Nano Lett.*, 2003, **3**, 373-378.